Research Square

Preprints are preliminary reports that have not undergone peer review.
They should not be considered conclusive, used to inform clinical practice,
or referenced by the media as validated information.

Impact of Nanoribbon Width on the Performance of Nanoscale Interconnects: A Material-Device-Circuit Co-modelling Approach

Shakti Kumar
Indian Institute of Information Technology
Kumar Gaurav
Madhav Institute of Technology & Science
Sandeep Pandey
University of Strathclyde
Boddepalli SanthiBhushan
sbhushan@iiita.ac.in

Indian Institute of Information Technology

Research Article

Keywords: Nanoscale Interconnect, Silicon Carbide, Nanoribbon, Fermi velocity, DFT, Delay

Posted Date: November 26th, 2026

DOI: https://doi.org/10.21203/rs.3.rs-11716561/v1

License: This work is licensed under a Creative Commons Attribution 4.0 International License.
Read Full License

Additional Declarations: No competing interests reported.

Impact of Nanoribbon Width on the Performance of Nanoscale Interconnects: A Material-Device-Circuit Co-modelling Approach

Shakti Kumar [1], Kumar Gaurav [2], Sandeep Pandey [3], Boddepalli SanthiBhushan [1*]

[1] Department of Electronics and Communication Engineering,

Indian Institute of Information Technology, Allahabad, UP 211015, India.

[2] Department of Electronics Engineering, Madhav Institute of Technology and Science, Gwalior, MP 474005, India.

[3] Department of Pure and Applied Chemistry, University of Strathclyde, Glasgow G1 1XQ, United Kingdom.

[*]e-mail: sbhushan@iiita.ac.in

ABSTRACT

This work reports an in-depth investigation to understand the width dependence of Zig-Zag Silicon Carbide Nanoribbon (ZZ-SiC NR) interconnect performance through DFT, NEGF, and Cadence Virtuoso EDA-based material-device-circuit co-modelling approach. The investigation is performed for three stable ZZ-SiC NR widths, N = 6, 8, and 10, as identified by MD simulations. The cohesive energy investigation revealed an increase in stability with the ribbon width, attributed to the reduced edge-to-bulk ratio and quantum confinement effects. All the ZZ-SiC NRs exhibit metallic behaviour with increasing states density with the ribbon width near Fermi level. The two-probe device analysis revealed that the drive current increases with the ribbon width, which can be attributed to the availability of a large channel area and significant forward transmission pathways.

The distributed parasitic elements, including quantum capacitance, increase with the ribbon width, while the kinetic inductance, magnetic inductance, and electrical resistance decrease. The driver-interconnect-load (DIL) circuit simulations reveal increased average power consumption with ribbon width, attributed to higher drive current. However, the delay and the power delay product (PDP) were found to decrease as ribbon width increased. The maximum frequency of operation (MFOO) is also found to increase with ribbon width, attributed to reduced delay. Thus, it is advised to choose a nanoribbon with a higher width possible, for greater interconnect performance. However, if the power dissipation is a major concern of the IC designer rather than delay, PDP, and MFOO, then it is advised to choose the least ribbon widths possible.

Keywords – Nanoscale Interconnect, Silicon Carbide, Nanoribbon, Fermi velocity, DFT, Delay.

1. INTRODUCTION

In general, materials can be categorized as 0D, 1D, 2D, or 3D based on their size in different dimensions and the quantum confinement [1]. Out of these, 2D and 1D materials find broader applications due to their fascinating structural stability, electronic, transport, and other properties, which are closely related to carrier confinement in one or more dimensions [2]. 2D materials have become a popular choice among researchers since the mechanical exfoliation of graphene in 2004 at the University of Manchester, followed by the subsequent confirmation of their superior properties [3-4]. Over the past few decades, significant emphasis is given for the analogues materials of graphene and their applications at reduced dimensions, including the transition-metal dichalcogenides (TMDs), silicene, germanene, stanene, phosphorene, etc. [5-8]. The dimensional

reduction of 2D Silicon carbide (SiC) to extract the 1D SiC can alter the electronic band nature of SiC from a wide-band-gap material to either a metallic or semiconducting one.

Interconnects are very thin and complex system of wirings used to facilitate communications among various components and their connection with power and ground railings on an IC, composed of metals or low-resistive non-metals, such as copper (Cu), aluminium (Al), gold (Au), polysilicon, silicides, and polycides, among others. These wirings connect multiple transistors or devices together via connections with the polysilicon gate and P^+/N^+ source-drain terminology. The slower transistor speed associated with larger channel size used to the major limiting factor to the performance of ICs in early generations, however as the transistor density and speed are greatly enhanced based on Moore's law in the subsequent generations, the thinner and closely interconnects significantly affect the IC performance [9- 11]. Broadly, interconnects are categorized into local and global, with metals preferred for global interconnects [12-16]. Due to the relatively smaller lengths of local interconnects, low-resistive non-metals such as polysilicon [17], silicides [18-19], and polycides [20] can be utilized for local interconnects. The use of non-metals for local interconnects provides several benefits, including improved process compatibility and a reduced threshold voltage of transistors, which stems from a smaller work function difference, among other advantages. The industry utilized aluminium as interconnect in earlier technologies, later replaced by copper in 1990s due to increased resistance and electromigration issues with the former. However, Cu also exhibits some drawbacks at the nanoscale, such as increased resistance due to a small mean free path [21-22]. The mean free path of electrons is influenced by multiple scattering effects, including grain boundary and side wall scattering, as well as electromigration. Due to this deficiency, the nanoscale alternatives made of nanoribbons, nanotubes, and nanowires are under extensive investigation.

Agrawal *et al.* reported the doping of [X= N, Al, P, B] at different positions from center to edge in the zig-zag Graphene nanoribbons (ZGNRs) for interconnect applications, and observed significant enhancement in performance metrics delay and PDP for nitrogen-doped ZGNR than its counterparts [23]. Agrawal *et al.* performed the DFT analysis on edge-engineered graphene nanoribbons and reported that both edge oxygen-passivated graphene nanoribbons offer better performance parameters and are suitable for interconnect applications [24]. The impact of multiple layers of a GNR on the interconncect performance is explored by Kaur *et al.* [25] and reported substantial improvement in interconnect performance in comparison to Copper. Fang *et al.* utilized edge passivation and doping to tune the properties of properties of zig-zag silicene nanoribbons (ZSiNR) [26]. Kharwar *et al.* utilized F and H edge passivation of SiNRs to tune the material properties and reported energetic favourability of F over H passivation [27]. GNR edge passivation with Pt, Ru, Rh and Pd are explored by Nishad *et al.* for nanoscale interconnects, and reported over 10 times better delay and 9 times better PDP for Ru passivation than H. [28]. Despite the availability of several reports, it is unclear from the literature how the nanoribbon width affects interconnect performance. Thus, this work aims to evaluate the width dependence of silicon carbide nanoribbons to enhance the performance of nanoscale interconnects. It is to be noted that SiC is a binary compound composed of alternating silicon and carbon atoms arranged in a hexagonal honeycomb lattice structure [29]. Due to the different atomic characteristics of Si and C, SiC exhibits partially ionic–covalent bonding with predominantly sp^2- type hybridization, in its planar configuration and has a finite energy gap, distinguishing it from gapless graphene [30-31]. However, the nanoribbons of SiC can be either metallic or semiconducting, depending upon the chirality and ribbon width.

2. COMPUTATIONAL DETAILS

The material and two-probe device properties are extracted using the density functional theory (DFT) and non-equilibrium Green's function (NEGF) formalisms based commercial code Synopsys-QuantumATK [32]. The Cadence Virtuoso Electronic Design Automation (EDA) tool is used to extract circuit performance metrics for the nanoscale interconnect. The material and device simulations utilize spin-polarized Generalized Gradient Approximation (SGGA) exchange-correlation functional, and the limited-memory Broyden-Fletcher-Goldfarb-Shanno (L-BFGS) algorithm [33] employed for structural relaxations to attain force and stress tolerances of $0.05\ eV/\text{Å}$, and $0.05\ eV/\text{Å}^3$, respectively. The designed ZZ-SiC NRs exhibit periodicity in the z-direction and confinement in the other two directions with sufficient vacuum padding of 15 Å. The convergence tests envisage a Monkhorst-Pack grid *k-point* sampling of $1 \times 1 \times 29$ for Brillouin zone sampling, and a density mesh cut-off of 160 Rydberg for all the considered structures. The atomic orbitals are defined using localized double-zeta polarised basis sets [34].

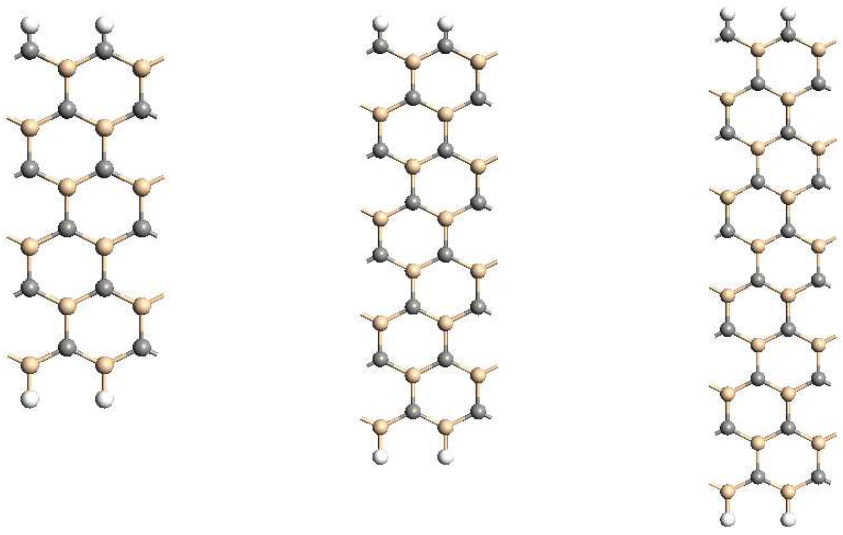

(a) (b) (c)

Fig. 1. Optimized geometries of ZZ-SiC NR of width (a) N=6, (b) N=8, and (c) N=10.

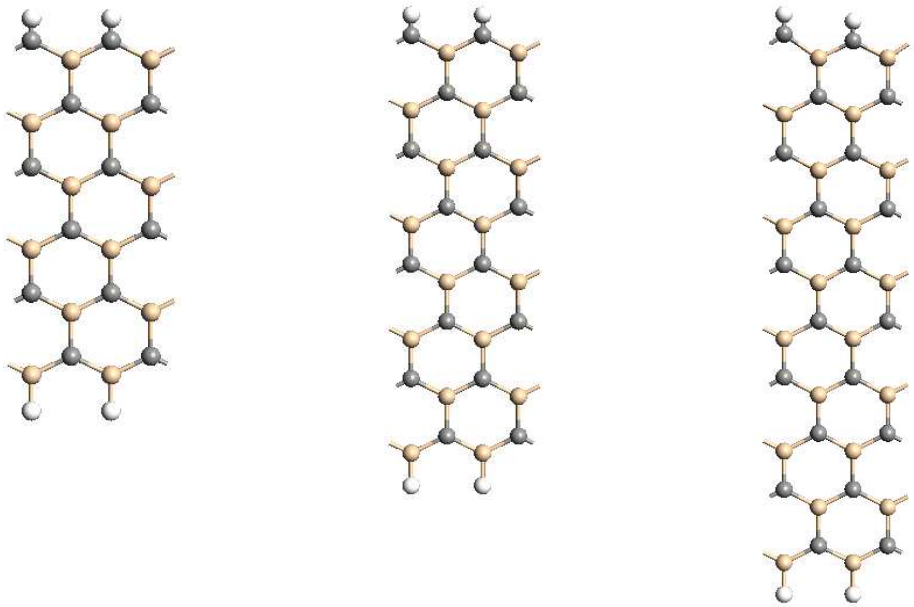

(a) (b) (c)

Fig. 2. ZZ-SiC NR geometries obtained from MD simulations after 5ps for (a) N=6, (b) N=8, and (c) N=10.

3. RESULTS AND DISCUSSION

3.1 Structural Aspects and Stability Investigation

The optimized Geometries of ZZ-SiC NR (N=6, 8, and 10) within the unit cell are depicted in **Fig. 1**. The structural aspects, such as the ribbon width, Si-C bond length, unit cell size in periodic direction, and cohesive energies, are tabulated in **Table 1.** The thermal stability and relative thermodynamic stability of the ZZ-SiC NRs are assessed with the help of molecular dynamics (MD) simulations and cohesive energy calculations, respectively. The MD simulations are performed up to 5ps with a step of 1fs using the Maxwell-Boltzmann initial velocity and NVT Berendsen ensemble. The structures obtained after a 5ps MD simulation are shown in **Fig. 2**, where the ZZ-SiC NRs exhibit greater stability, regardless of their width. Moreover, to identify the energetically preferred magnetic configuration, the ZZ-SiC NRs are investigated using total energy calculations for the non-magnetic (NM), ferromagnetic (FM), and antiferromagnetic (AFM) spin configurations via initialization at the nanoribbon edge spin states. In general, the spin polarization in zig-zag nanoribbons originates from the localized edge states and influences the electronic structure. The edge atoms exhibit the strongest spin polarization, which gradually decreases toward the central region of the ribbon. Our simulations reveal that AFM state exhibits the lowest energy for N=6 and N=8, whereas FM state exhibits lowest total energy for N=10, hence are considered in further simulations. The Cohesive energy (E_{coh}) per atom is also assessed utilizing the expression [35],

$$E_{coh} = \frac{(E_{total} - m * E_H - n * E_C - p * E_{si})}{m + n + p} \qquad (1)$$

Here, E_{total} is the energy of the passivated ZZ-SiC NR structure, E_{Bare} is the energy of the structure without passivation, E_H , E_C , and E_{si} is the energy of the single hydrogen, carbon and silicon atom, respectively, and m, n and p are the no of hydrogen, carbon and silicon atoms, respectively. Generally, a lower cohesive energy corresponds to greater thermodynamic stability, and a negative value indicates an exothermic nature. From **Table 1**, the cohesive energy decreases with increasing ribbon width, indicating increased stability as ribbon width increases. This can be attributed to the reduced edge-to-bulk ratio and quantum confinement effects. The ZZ-SiC NR (N=10) is the relatively most stable configuration with a cohesive energy of -5.74 eV, while the ZZ-SiC NR (N=6) is relatively the least stable configuration with a cohesive energy of -5.55 eV. The order of stability according to cohesive energy is ZZ-SiC NR (N=10) > ZZ-SiC NR (N=8) > ZZ-SiC NR (N=6).

Table 1. Structural and Electronic Aspects of ZZ-SiC NRs for different widths.

Nanoribbon Size (N)	Nanoribbon Width (Å)	Unit Cell Length (Å)	Si-C Bond Lengths (Å)	Cohesive Energy (eV)	Electronic Nature	Fermi velocity (m/s)
6	16.37	6.51	1.80	-5.55	Metallic	1.28×10^5
8	21.78	6.51	1.80	-5.65	Metallic	1.57×10^5
10	27.13	6.51	1.80	-5.74	Metallic	4.56×10^4

3.2 Electronic Properties of the ZZ-SiC NRs

Following confirmation of the structural stability of the ZZ-SiC NRs, we proceed to investigate their electronic properties using spin-polarised band structure and density of states (DOS) profiles (see **Fig. 3**), where the Fermi energy is set to zero. In the presented profiles, black and red curves

represent spin-up and spin-down states, respectively. The presence of electronic states at Fermi energy level indicates the metallic behaviour of ZZ-SiC NRs. Moreover, increasing state density is observed at the Fermi level with ribbon width for both spin orientations [36]. In general, metallicity is a necessary condition for a material to be used a global interconnect. Furthermore, the Fermi velocity (V_F) of the ZZ-SiC NRs is manually extracted from the electronic band structures using,

$$V_F = \frac{1}{\hbar}\frac{dE}{dk} \qquad (2)$$

The Fermi velocity of ZSiNRs follows the pattern ZZ-SiC NR (N=10) < ZZ-SiC NR (N=6) < ZZ-SiC NR (N=8).

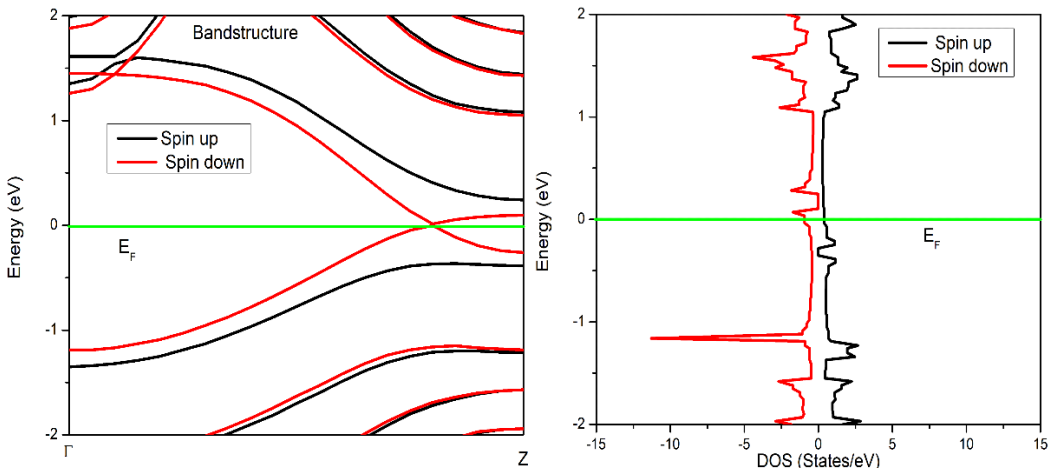

(a)

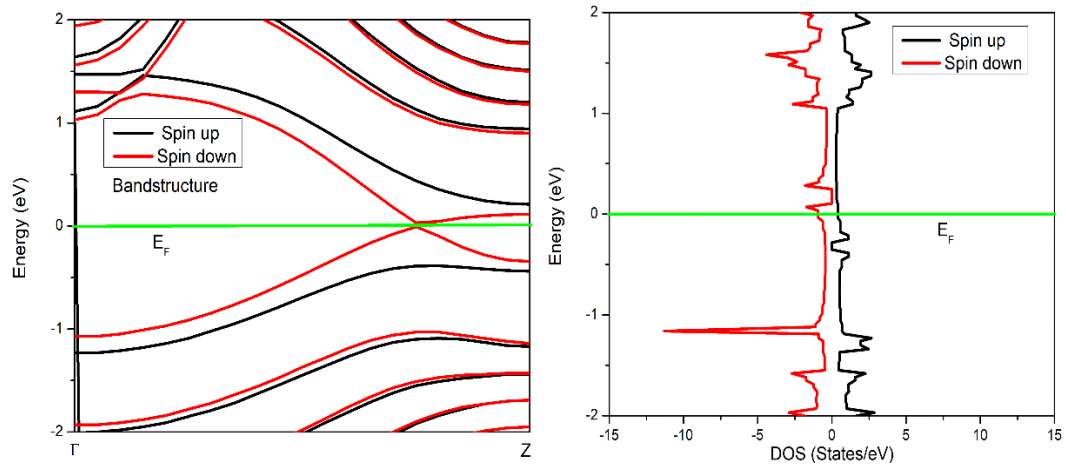

(b)

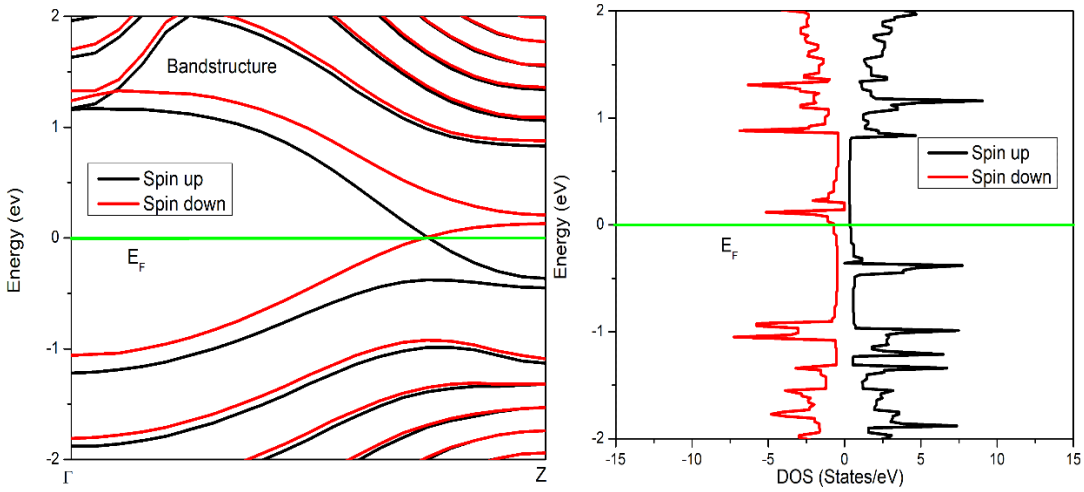

(C)

Fig. 3. Spin-polarised E-K diagrams and DOS profiles of ZZ-SiC NRs having (a) N=6, (b) N=8, and (c) N=10.

3.3 Two-probe Device Analysis

The two-probe device analysis is performed to extract the current-voltage (I-V) characteristics, the transmission Eigen values (N_{ch})/number of conduction channels, and the transmission pathways.

The sample two-probe device setup for N=6 is depicted in **Fig.4**, which contains a central scattering region and two electrodes (left and right). The advanced and retarded green's functions ($G^{A}(E)$, and $G^{R}(E)$), and the left and right electrode coupling coefficients with the channel region ($\Gamma^{L}(E,V)$, and $\Gamma^{R}(E,V)$) are used to extract the transmission coefficients, which are used within the Landauer-Buttiker formula along with the Fermi function difference to extract the current-voltage characteristics [38].

$$T(E,V) = T_r\,[\,\Gamma^{L}(E,V)G^{R}(E)\Gamma^{R}(E,V)G^{A}(E)] \quad (3)$$

$$I = \frac{2e}{h}\int_{-\infty}^{\infty} T(E,V)[f\left(\frac{E-\mu_L}{k_B T_L}\right) - f\left(\frac{E-\mu_R}{k_B T_R}\right)]\,dE \qquad [39] \qquad (4)$$

Here, $E-\mu_R$ and $E-\mu_L$ are the energies with respect to their chemical potentials of the right and left electrodes, respectively. k_B and h are the Boltzmann's and Planck's constants, respectively. e is the electronic charge, and T is the temperature.

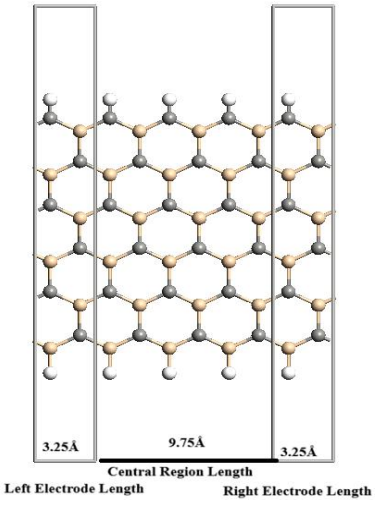

Fig. 4. Two-probe model of ZZ-SiC NR (N=6).

The computed I-V curves of all the ZZ-SiC NRs are plotted in **Fig. 5,** where the drive currents noted at a bias voltage of 1V follow the pattern as ZZ-SiC NR (N=10) > ZZ-SiC NR (N=8) > ZZ-SiC NR (N=6), with ZZ-SiC NR (N=10) offering the highest current of about 155 μA, and ZZ-SiC NR (N=6) offering the least current of about 94.90 μA. To understand the reason behind the increase in current with respect to the ribbon width, the transmission pathways have been examined (see **Fig. 6**). Here, the blue and red arrows indicate forward transmission pathways and reverse transmission pathways, respectively, while the green arrows indicate scattered transmission. ZZ-SiC NR (N = 6) has significant forward transmission in the channel; however, overall transport is hampered by strong scattering and reverse transmission at the edges. As the ribbon width increases, the scattering and reverse transmission at the edges become stronger, yet the availability of a larger channel area and numerous forward transmission pathways boost the overall current flow between the electrodes. The currents calculated at an applied potential of 1V are utilized to extract the distributed electrical resistance R (in MΩ/μm), and tabulated in **Table 2.** The table also lists the number of conduction channels or transmission eigenvalues (N_{ch}) extracted from the transmission matrix [40]. N_{ch} indicates the number of transmission paths available for an electron to move from one end to the other end of the device without undergoing scattering, at a given potential. It has a critical role in estimating the distributed/dynamical parameters of the ZZ-SiC NR interconnects.

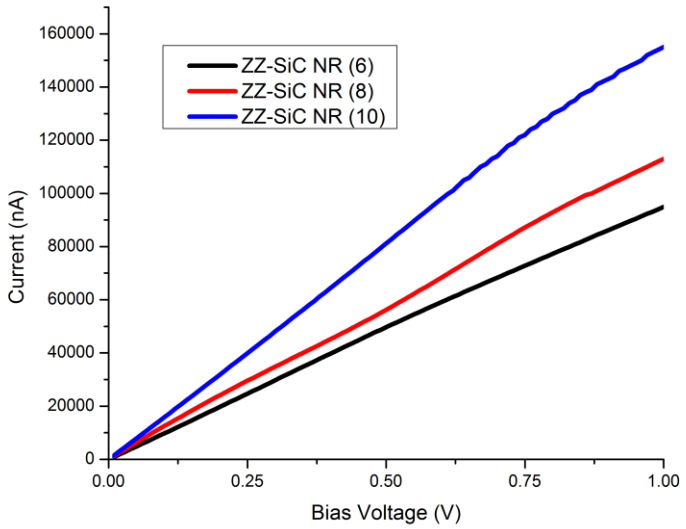

Fig. 5. I-V curves obtained for the ZZ-SiC NRs (N = 6, 8, and 10).

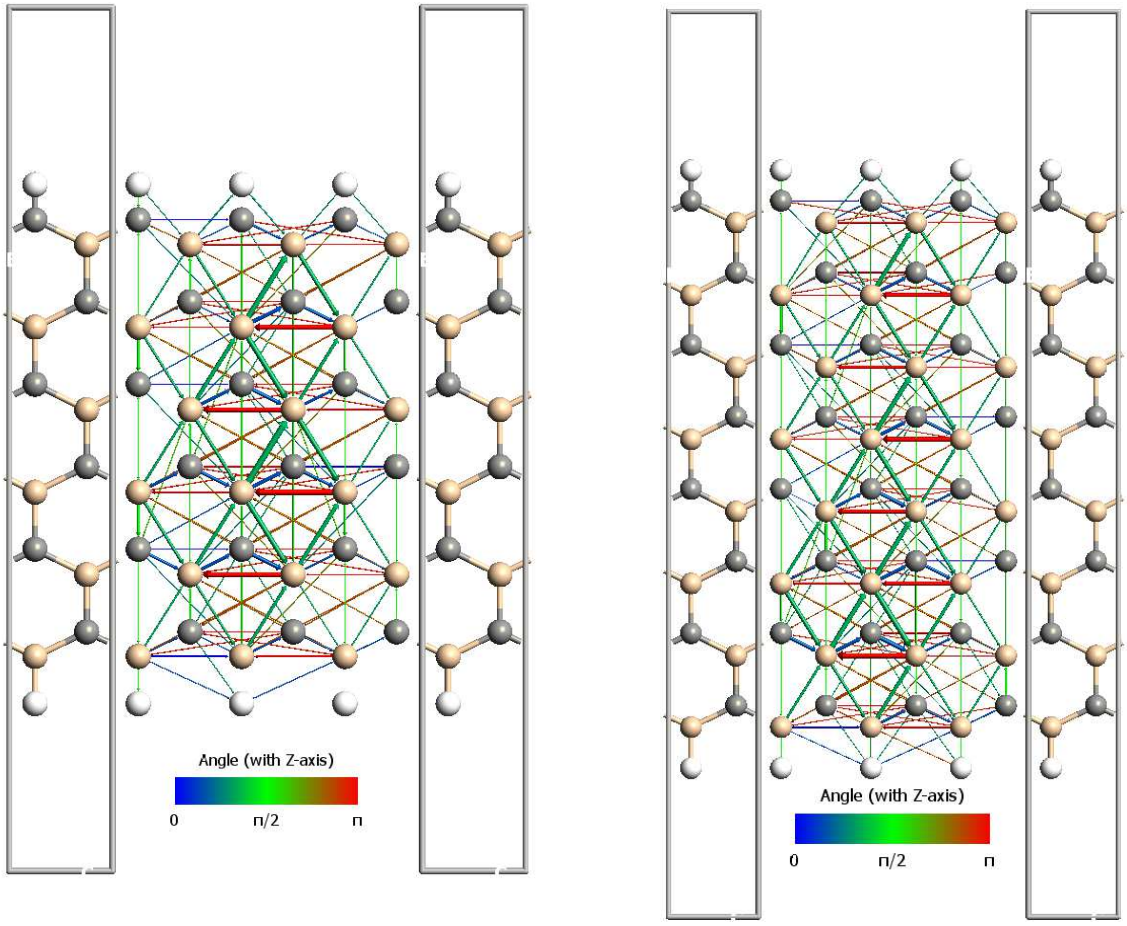

(a) (b)

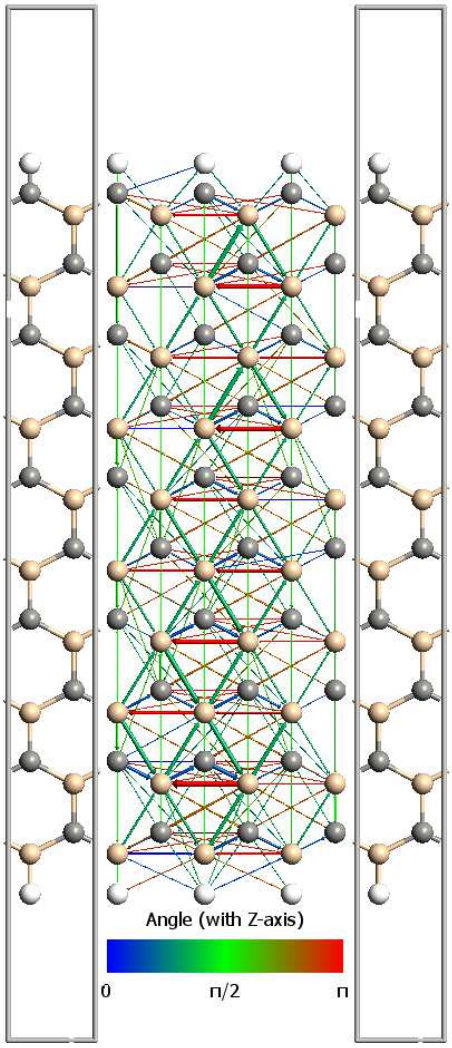

(c)

Fig. 6. Transmission pathways for ZZ-SiC NRs having (a) N=6, (b) N=8, and (C) N=10.

3.4 Dynamical Parameters

The material and 2-probe device analysis results are utilized to calculate the various distributed/dynamical parameters of the nanoscale interconnect, namely Quantum capacitance (C_Q), Kinetic inductance (L_K), Electrostatic capacitance (C_E), Magnetic inductance (L_M), and Quantum resistance (R_Q), assuming the interconnect is surrounded by a perfect dielectric. The conventional model of interconnect includes only three dynamical elements viz. electrical resistance (R) - resistance to the current flow, electrostatic capacitance (C_E) - ability to store the charge electrostatically, and magnetic inductance (L_M) – ability to store energy in the form of magnetic field. On the other hand, the nanoscale model of interconnect includes another three dynamical elements viz. the quantum resistance (R_Q), quantum capacitance (C_Q), and kinetic inductance (L_K), along with R, C_E and L_M. These parameters become prominent at the nanoscale due to the low density of states and the quantum effects.

The quantum resistance (R_Q) is the inverse of conductance quantum (G_Q), represents the conductance of a single channel with transmission probability of 1, i.e. no scattering. The quantum resistance for our ZZ-SiC NRs is estimated by dividing the fundamental unit of resistance with the number of transmission Eigen values (N_{ch}) available for different ribbon widths.

$$R_Q = \frac{1}{G_Q} = \frac{h}{2e^2}\frac{1}{N_{ch}} \qquad (5)$$

The electrostatic capacitance (C_E) indicates the fringe-field coupling between the nanoribbon interconnect and the ground or substrate through the surrounding dielectric, characterizing the purely geometric contribution to the overall charge-storage capability of the nanoscale interconnect. The magnetic inductance (L_M) represent the ability of material to store the energy in the form of magnetic field. In the early stages of IC design, the influence of L_M can be neglected due to the low frequency of clock/signals, given the fact that the impedance offered by the inductance is directly proportional to the signal frequency. However, in the advanced ICs with clock frequencies reaching a few GHz's, the impact of L_M cannot be neglected anymore.

$$C_E = \frac{2\,\pi\varepsilon}{\ln\frac{y}{w}} \qquad (6)$$

$$L_M = \frac{\mu}{2\pi}\ln\frac{y}{w} \qquad (7)$$

Here μ and ε are the permeability and permittivity of the dielectric surrounding of the nanoribbon interconnect (vacuum in our case [41-43]), respectively. y is the distance from the ground or substrate (1 μm in our case) and w is the width of the nanoribbon.

The quantum capacitance (C_Q) is associated with the rapid charge variations in the nanoscale interconnect when a potential is applied, due to the low density of states. The kinetic inductance arises from the inertia associated with the carriers when used to carry time-varying or alternating signals.

$$C_Q = \frac{(4e^2)}{hv_f}\ N_{ch} \qquad (8)$$

$$L_K = \frac{h}{4e^2\ v_f}\frac{1}{N_{ch}} \qquad (9)$$

The calculated dynamical parameters or distributed parasitic elements of the ZZ-SiC NRs are listed in **Table 2**, where a comparison with previous reports is also provided. The values reported in this work are in qualitative agreement with the previously reported data for interconnects.

As seen from **Table 2**, R and L_M decrease with increasing ribbon width, as the increased ribbon width cause less opposition to the current and change in current. C_E increases with the ribbon width due to the large electrostatic coupling with the substrate or ground. C_Q increases with the ribbon width due to the increased state density near the Fermi level (see **Fig.3**). The decrease in L_K with ribbon width can be attributed to the increase of N_{ch} with increased ribbon width (see **Table 2**). In general, the parameters R, C_E, L_M, R_Q, C_q and L_K should be as low as possible for better performance of the interconnect. Here, no particular width possesses the lowest values of all the dynamical parameters. ZZ-SiC NR (N=16) has the lowest values of R_Q, R, L_M, $C_{,Q}$ and L_K ,ZZ-SiC NR (N=8) has the lowest value of C_E. Thus, it is impossible to reach any conclusion as to how the nanoribbon width is impacting the performance of the interconnect. Therefore, we proceed to the simulation of the distributed circuit model of the nanoscale interconnect in the next section.

Table 2. Comparison of the distributed/dynamical elements and number of conduction channels (N_{ch}) of ZZ-SiC NR interconnects.

Material	**N_{ch}**	**R_Q (kΩ)**	**L_K (μH/μm)**	**C_Q (pF/μm)**	**C_E (aF/ μm)**	**L_M (pH/ μm)**	**R (MΩ/μm)**
ZZ-SiC NR (N=6)	5	2.58	0.024	0.014	8.67	1.28	6.48
ZZ-SiC NR (N=8)	6	2.15	0.021	0.018	9.08	1.22	4.06

ZZ-SiC NR (N=10)	9	1.43	0.020	0.0039	9.42	1.18	2.37
P-ZGNR [23]	3	4.30	0.14	0.031	-	-	-
O-ZGNR-O [24]	3	4.30	0.010	0.0022	8.46	1.31	-
ZSiNR [35]	3	4.30	0.14	31.97	-	-	-
Bare ZGaNNR [44]	3	4.30	0.48	0.15	-	-	-
H-ZnONR [45]	2	6.46	0.27	0.026	-	-	-

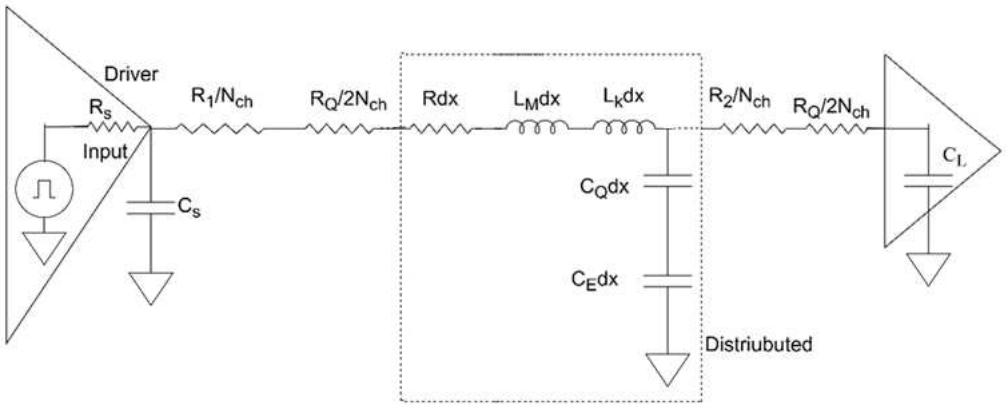

Fig. 7. Driver- interconnect -load (DIL) model.

Table 3. Various essential parameters considered for the circuit analysis.

Parameters	Value
Dielectric constant (ε_r)	1
Additional contact resistance per channel, R_1, R_2 ($k\Omega$) [28]	4.3
Driver resistance, R_s ($k\Omega$) [28]	41
Driver capacitance, C_s (aF)	3.5
Load capacitance, C_L(aF)	3.5
Supply voltage (V)	2

3.5 Circuit Analysis

The DIL system shown in **Fig. 8,** is simulated for circuit analysis by varying the interconnect length in each simulation. The dynamical parameters and other crucial parameters utilised for the DIL system are presented in **Table II** and **Table III**, respectively. The circuit parameters for digital applications are plotted in **Fig. 8**.

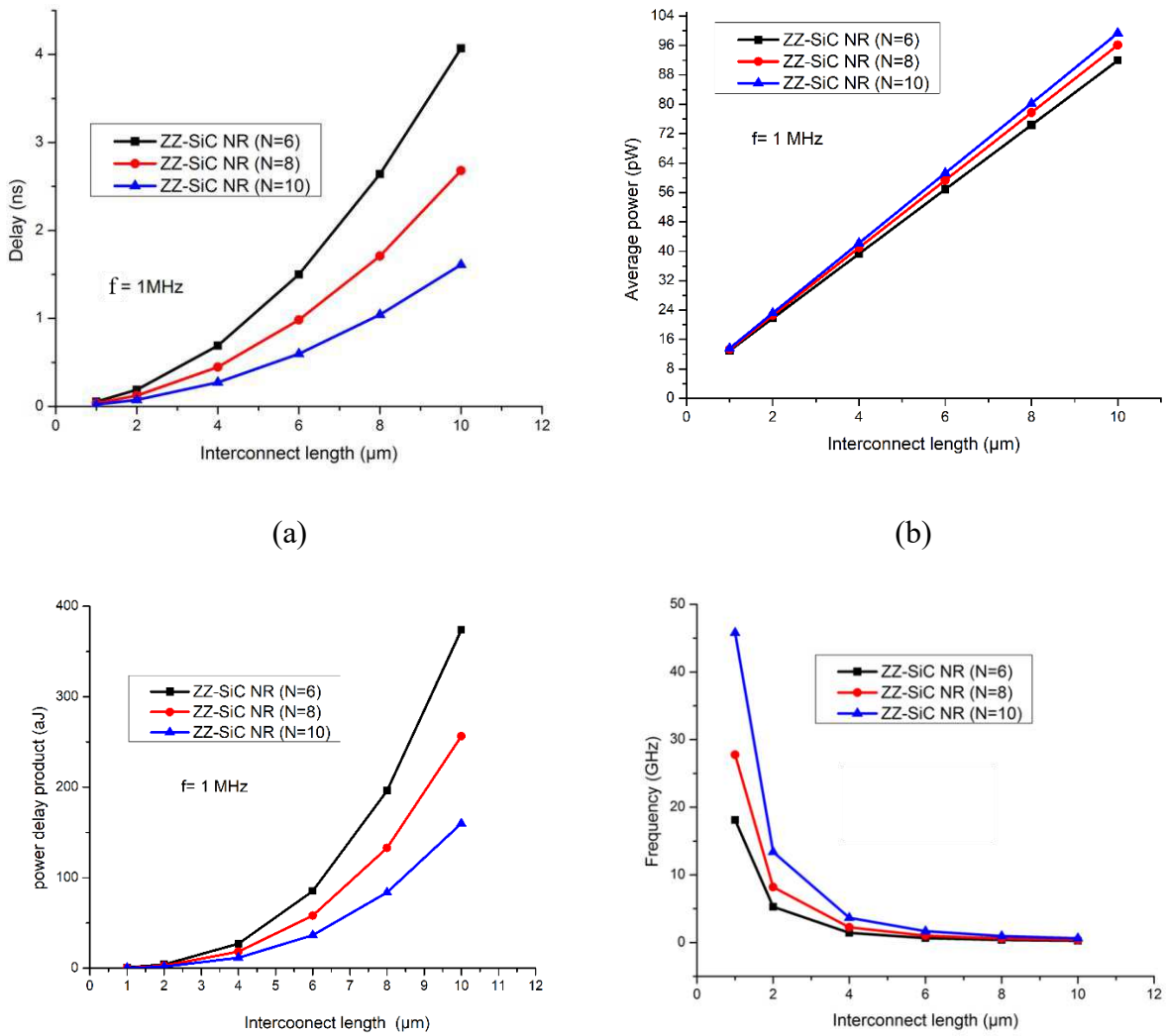

Fig. 8. (a) Delay, (b) Average power, (c) power delay product, and (d) Maximum Frequency of operation for digital applications w.r.t interconnect length.

Based on simulation results, the ZZ-SiC NR (N=10) interconnect exhibited superior performance for an interconnect length of 1 μm at a frequency of 1 MHz, achieving the minimum propagation delay, lowest PDP, and the maximum frequency of operation for digital applications compared to the other two widths (N=6 and N=8), However, the average power is higher for the ZZ-SiC NR (N

= 10), which can be attributed to the relatively higher drive currents arising from the improved edge-to-bulk ratio (see **Fig. 5**). For all the interconnect lengths ($1\mu m$- $10\mu m$), the propagation delay is found to increase non-linearly, maintaining the pattern ZZ-SiC NR (N=10) < ZZ-SiC NR (N=8) < ZZ-SiC NR (N=6) (see **Fig. 8a**). The delay offered by ZZ-SiC NR (N=10) for $1\mu m$ interconnect length (21.84 pS) is 1.64 times lesser than ZZ-SiC NR (N=8) and 2.52 times less than ZZ-SiC NR (N=6). This delay is quite lower than the previously reported delay of 26.3μs for Cu-doped ZZ boron nitride NR interconnects [46], 42.17μs for F-passivated ZZ GNR interconnects [47], and in good agreement with the delay reported for global interconnect copper (36.2 ps/μm) after incorporation of width-dependent scattering at 5nm technology node [48].

The average power has been plotted in **Fig. 8b** w.r.t interconnect length, which increases linearly with the length of interconnect. At a length of 1μm, the ZZ-SiC NR (N=10) offers the highest power of 13.60 pW, followed by ZZ-SiC NR (N=8) 13.32 pW and ZZ-SiC NR (N=6) 12.94 pW. While the delay decreased with increase in ribbon width, the average power increased with the ribbon width indicating lower power dissipation at smaller ribbon widths. This increase in power dissipation with ribbon width can be attributed to the increase in drive currents (see **Fig.5**). The average power dissipated by the ZZ-SiC NR (N=8) is significantly lower than the previously reported power dissipation in μW for the zig-zag Zinc oxide nanoribbon interconnects [42].

For better circuit performance, it is crucial to have a lower PDP. The analysis of PDP (see **Fig. 8c)** reveals decreasing PDP with increasing ribbon width. ZZ-SiC NR (N=10) offers the lowest PDP of 0.29 zJ, followed by ZZ-SiC NR (N=8) 0.47 zJ, and ZZ-SiC NR (N=6) 0.77 zJ at an interconnect length of 1μm. The PDP is observed to increase non-linearly with length, upholding the pattern: ZZ-SiC NR (N = 10) < ZZ-SiC NR (N = 8) < ZZ-SiC NR (N = 6) for all lengths. The power-delay

product offered by these ribbons is significantly lower than the previously reported PDP in fJ for zig-zag Zinc oxide nanoribbons interconnects [42].

Moreover, the MFOO of the interconnect is calculated for the purpose of digital ICs (see **Fig. 8d**). For an interconnect length of $1\mu m$, ZZ-SiC NR (N=10) offers the highest MFOO of 45.78 GHz, followed by ZZ-SiC NR (N=8) 27.77 GHz, and ZZ-SiC NR (N=6) 18.11 GHz. As the interconnect length increases from $1\mu m$ to $10\mu m$, the MFOO is observed to decrease non-linearly with increasing length, upholding the pattern ZZ-SiC NR (N = 10) > ZZ-SiC NR (N = 8) > ZZ-SiC NR (N = 6) for all lengths. Thus, the MFOO is found to increase with the ribbon width regardless of the interconnect length.

To conclude the circuit analysis, the overall performance of ZZ-SiC NR interconnect is found to improve as the ribbon width is increased, thus it is advised to choose the larger ribbon widths possible for the better performance of interconnect. The ZZ-SiC NR (N=10) offered the lowest propagation delay, highest MFOO, and lowest PDP, despite offering higher power dissipation than the N=10 and N=6 widths. However, if the IC area and average power dissipation are the critical concerns of an IC designer rather than the delay, MFOO and PDP, then it is advised to go with the lowest possible ribbon widths for interconnects.

4. CONCLUSION

The DFT, NEGF, and Cadence Virtuoso EDA based material-device-circuit co-modelling approach is utilized to understand the impact of nanoribbon width on the performance of nanoscale interconnects. The investigation is performed on three stable ZZ-SiC NR widths, N = 6, 8, and 10, as identified through the MD simulations. The Cohesive energy investigation revealed an increase in stability with the ribbon width, attributed to the reduced edge-to-bulk ratio and quantum

confinement effects. All the ZZ-SiC NRs exhibit a metallic nature, irrespective of width; however, an increased state density is observed near the Fermi level with increasing ribbon width. The two-probe device analysis revealed that the drive current increases with the ribbon width, which can be attributed to the availability of a large channel area and significant forward transmission pathways. The distributed parasitic elements, including kinetic inductance, quantum capacitance, and electrostatic inductance, increase with the ribbon width, while the magnetic inductance and electrical resistance decrease with increasing ribbon width. The DIL circuit simulations reveal that the average power consumption increases with the ribbon width, attributed to the increased drive current. However, the delay and PDP were found to decrease with increasing ribbon width. The MFOO is also found to increase with the ribbon width, attributed to the reduced delay. Thus, it is advised to choose a nanoribbon with a higher width possible, for greater interconnect performance. However, if the power dissipation is a major concern of the IC designer rather than delay, PDP, and MFOO, then it is advised to choose the least ribbon widths possible.

Acknowledgement:

The author BS is thankful to Indian Institute of Information Technology Allahabad for providing the computational resource under the Seed Research Grant vide no. I1ITA/RO/1532/2022.

Conflict of Interest:

The authors have no known conflict of interests to declare.

AI Usage:

This work doesn't use any AI tool for data generation and writing.

Data statement:

No datasets are used to perform the present work.

Funding Information:

Funding is not available for this particular work.

Author contributions:

S.K. – Investigation, Formal Analysis, Writing – original draft.

K.G. – Formal Analysis, Writing – original draft.

S.P. – Methodology, Writing – review and editing.

B.S. – Conceptualization, Methodology, Supervision, Writing – review and editing.

REFERENCES

[1]. Liu, Yulian, Yi Wei, and Zewei Quan. "Regulating Circularly Polarized Luminescence in Zero-Dimensional Chiral Hybrid Metal Halides." *Accounts of Materials Research* 6, no. 5 (2025): 638-647.

[2]. Wang, Bing, James Iocozzia, Meng Zhang, Meidan Ye, Shicheng Yan, Huile Jin, Shun Wang, Zhigang Zou, and Zhiqun Lin. "The charge carrier dynamics, efficiency and stability of two-dimensional material-based perovskite solar cells." *Chemical Society Reviews* 48, no. 18 (2019): 4854-4891.

[3]. Haider, Ali, Muhammad Farooq Rasheed, Amna Abrar, Aisha Mumtaz, Aneesa Zeb, Maneeb Ur Rehman, Ghulam Mujtaba Noor, and Shahid Ashraf. "THE CHEMISTRY OF 2D MATERIALS FROM GRAPHENE TO BEYOND." *Kashf Journal of Multidisciplinary Research* 2, no. 01 (2025): 197-221.

[4]. Goel, Neeraj, and Rahul Kumar. "Physics of 2D materials for developing smart devices." *Nano-Micro Letters* 17, no. 1 (2025): 197.

[5]. Grazianetti, Carlo, Alessandro Molle, and Christian Martella. "The future of Xenes beyond graphene: challenges and perspective." *2D Materials* 11, no. 4 (2024): 042005.

[6]. Radhakrishnan, Sidharth, Partha Pratim Das, Aszad Alam, Shashi Prakash Dwivedi, and Vijay Chaudhary. "Mechanical, thermal, and electrical properties of 2D nanomaterials for advanced applications." *Proceedings of the Institution of Mechanical Engineers, Part C: Journal of Mechanical Engineering Science* 238, no. 17 (2024): 8739-8755.

[7]. Aditya, D. S., and S. K. Nataraj. "Structural, Optical, and Electronic Properties of Two-Dimensional Nanomaterials." *Two-Dimensional Nanomaterials-Based Polymer Nanocomposites: Processing, Properties and Applications* (2024): 167-194.

.

[8]. Thakur, Shilpa, Pandian Mannu, Chung-Li Dong, Senthil Kumar Muthusamy, and Asokan Kandasami. "Recent Progress and Developments in Transition Metal Dichalcogenides: Synthesis, Properties, and Applications." *The Chemical Record* (2025): 2400245.

[9]. Kumbhare, Vijay Rao, Rahul Kumar, Manoj Kumar Majumder, Somesh Kumar, Punya Prasanna Paltani, Brajesh Kumar Kaushik, and Rohit Sharma. "High-speed interconnects: history, evolution, and the road ahead." *IEEE Microwave Magazine* 23, no. 8 (2022): 66-82.

[10]. Lu, Ping-Jing, Ming-Che Lai, and Jun-Sheng Chang. "A survey of high-performance interconnection networks in high-performance computer systems." *Electronics* 11, no. 9 (2022): 1369.

[11]. Wu, Yuqi, and Zhongliang Pan. "Time-domain response improvement and bandwidth expansion of graphene nanoribbon interconnects using two types of high-k dielectric materials." *Journal of Computational Electronics* 24, no. 6 (2025): 1-18.

[12]. Zou, Yong Sheng, Chong Leong Gan, Min-Hua Chung, and Hem Takiar. "A review of interconnect materials used in emerging memory device packaging: first-and second-level interconnect materials." *Journal of Materials Science: Materials in Electronics* 32, no. 23 (2021): 27133-27147.

[13]. Rosenberg, R., D. C. Edelstein, C-K. Hu, and K. P. Rodbell. "Copper metallization for high performance silicon technology." *Annual review of materials science* 30, no. 1 (2000): 229-262.

[14]. Timakov, A. V., V. S. Gornostay-Polsky, and V. I. Shevyakov. "Multilevel Metallization of High-Temperature Silicon ICs Based on Tungsten. Physics and Technology: A Review." *Russian Microelectronics* 53, no. 7 (2024): 650-658.

[15]. Yan, Han, Xinhuan Niu, Minghui Qu, Fu Luo, Ni Zhan, Jianghao Liu, and Yida Zou. "A review: research progress of chemical–mechanical polishing slurry for copper interconnection of integrated circuits." *The International Journal of Advanced Manufacturing Technology* 125, no. 1 (2023): 47-71.

[16]. Castillo, Ezer, Michael Njuki, Abdullah Faisal Pasha, and Nikolay Dimitrov. "Copper-based nanomaterials for fine-pitch interconnects in microelectronics." *Accounts of Chemical Research* 56, no. 12 (2023): 1384-1394.

[17]. Xia, Qianfu, Xinrui Zhang, Binghe Ma, Kai Tao, Hemin Zhang, Weizheng Yuan, Seeram Ramakrishna, and Tao Ye. "A State-of-the-Art Review of Through-Silicon Vias: Filling Materials, Filling Processes, Performance, and Integration." *Advanced Engineering Materials* 27, no. 1 (2025): 2401799.

[18]. Mann, Randy W., Larry A. Clevenger, Paul D. Agnello, and Francis R. White. "Silicides and local interconnections for high-performance VLSI applications." *IBM Journal of Research and Development* 39, no. 4 (1995): 403-417.

[19]. Moon, Jun Hwan, Eunjin Jeong, Seunghyun Kim, Taesoon Kim, Eunsoo Oh, Keun Lee, Hauk Han, and Young Keun Kim. "Materials quest for advanced interconnect metallization in integrated circuits." *Advanced Science* 10, no. 23 (2023): 2207321.

[20]. Timakov, A. V., V. S. Gornostay-Polsky, and V. I. Shevyakov. "Multilevel Metallization of High-Temperature Silicon ICs Based on Tungsten. Physics and Technology: A Review." *Russian Microelectronics* 53, no. 7 (2024): 650-658.

[21]. Kim, Hyung-Woo. "Recent trends in copper metallization." *Electronics* 11, no. 18 (2022): 2914.

[22]. Li, Hong, Chuan Xu, Navin Srivastava, and Kaustav Banerjee. "Carbon nanomaterials for next-generation interconnects and passives: Physics, status, and prospects." *IEEE Transactions on electron devices* 56, no. 9 (2009): 1799-1821.

[23]. Agrawal, Sonal, Anurag Srivastava, and Gaurav Kaushal. "Performance metrics of doped graphene nanoribbons based nanoscale interconnects: DFT and NEGF analysis." *Solid State Communications* 380 (2024): 115389.

[24]. Agrawal, Sonal, Anurag Srivastava, Gaurav Kaushal, and Ashok Srivastava. "Edge engineered graphene nanoribbons as nanoscale interconnect: DFT analysis." *IEEE Transactions on Nanotechnology* 21 (2022): 43-51.

[25]. Kaur, M., N. Gupta, and A. K. Singh. "Performance analysis of multilayer graphene nanoribbon based interconnects." In *2017 IEEE MTT-S International Microwave and RF Conference (IMaRC)*, pp. 1-5. IEEE, 2017.

[26]. Fang, Dang-Qi, Sheng-Li Zhang, and Hu Xu. "Tuning the electronic and magnetic properties of zigzag silicene nanoribbons by edge hydrogenation and doping." *RSC advances* 3, no. 46 (2013): 24075-24080.

[27]. Kharwar, Saurabh, Sangeeta Singh, and Neeraj K. Jaiswal. "Structural & electronic properties of zigzag silicene nanoribbons with symmetric/asymmetric edge passivations via fluorine and hydrogen." *Physica B: Condensed Matter* 615 (2021): 413072.

[28]. Nishad, Vipul Kumar, Atul Kumar Nishad, Brajesh Kumar Kaushik, and Rohit Sharma. "First-principle analysis of transition metal edge-passivated armchair graphene nanoribbons for nanoscale interconnects." *IEEE Transactions on Nanotechnology* 20 (2021): 92-98.

[29]. S. A. Kukushkin and A. V. Osipov, “Epitaxial silicon carbide on silicon. Method of coordinated substitution of atoms (a review),” *Russ. J. Gen. Chem.*, vol. 92, no. 4, pp. 584–610, 2022.

[30]. M. M. Uddin, M. H. Kabir, M. A. Ali, M. M. Hossain, M. U. Khandaker, S. Mandal, A. Arifutzzaman, and D. Jana, “Graphene-like emerging 2D materials: Recent progress, challenges and future outlook,” *RSC Adv.*, vol. 13, no. 47, pp. 33336–33375, 2023.

[31] K. Emtsev, *Electronic and Structural Characterizations of Unreconstructed SiC {0001} Surfaces and the Growth of Graphene Overlayers*, Ph.D. dissertation, Friedrich-Alexander-Universität Erlangen-Nürnberg, Germany, 2009.

[32]. Stradi, Daniele, Umberto Martinez, Anders Blom, Mads Brandbyge, and Kurt Stokbro. "General atomistic approach for modeling metal-semiconductor interfaces using density functional theory and nonequilibrium Green's function." *Physical Review B* 93, no. 15 (2016): 155302.

[33]. Liu, Dong C., and Jorge Nocedal. "On the limited memory BFGS method for large scale optimization." *Mathematical programming* 45, no. 1 (1989): 503-528.

[34] da Silva, C. A. B., S. M. Côrrea, JC da S. dos Santos, K. R. Nisioka, M. Moura-Moreira, Y-P. Wang, J. Del Nero, and H-P. Cheng. "Topological insulator-metal transition and molecular electronics device based on zigzag phagraphene nanoribbon." *Journal of Applied Physics* 124, no. 8 (2018).

[35]. Agrawal, Sonal, Anurag Srivastava, and Gaurav Kaushal. "Density Functional Insight on Transport phenomenon in Halogenated Germanene and Silicene nanoribbons under tensile stress for nanoscale interconnects." *Micro and Nanostructures* (2025): 208300.

[36] Duarte, Jonas Marinho, Júlio César da Silva dos Santos, Denner Felipe Silva Ferreira, Carlos Alberto Brito da Silva Jr, and Jordan Del Nero. "Metallic Net-t Nanoribbons for Nanoelectronics: Width Modulation of NDR, Quasi-Ohmic Behavior, and Resonant Tunneling." *Surfaces and Interfaces* (2025): 108242.

[37]. Lang, Peter F. "Fermi energy, metals and the drift velocity of electrons." *Chemical Physics Letters* 770 (2021): 138447.

[38]. Smidstrup, Søren, Troels Markussen, Pieter Vancraeyveld, Jess Wellendorff, Julian Schneider, Tue Gunst, Brecht Verstichel et al. "QuantumATK: an integrated platform of electronic and atomic-scale modelling tools." *Journal of Physics: Condensed Matter* 32, no. 1 (2019): 015901.

[39]. Duarte, Jonas Marinho, Denner Felipe Silva Ferreira, Carlos Alberto Brito da Silva, and Jordan Del Nero. "2D chiral and armchair edges carbon allotrope nanoribbons: robust metallicity and tunable negative differential resistance in net-τ." *Nanoscale* 17, no. 47 (2025): 27382-27406.

[40]. Ceja Ayala, Rafael, Isaac Harris, Andreas Kleefeld, and Nikolaos Pallikarakis. "Analysis of the transmission eigenvalue problem with two conductivity parameters." *Applicable analysis* 103, no. 1 (2024): 211-239.

[41]. Chiang, C. K., H. Pai, J. L. Lin, J. K. Chang, M. Y. Lee, E. R. Hsieh, K. S. Li, G. L. Luo, Osbert Cheng, and S. S. Chung. "Finfet plus: A scalable finfet architecture with 3d air-gap and air-

spacer toward the 3nm generation and beyond." In *2021 International Symposium on VLSI Technology, Systems and Applications (VLSI-TSA)*, pp. 1-2. IEEE, 2021.

[42]. Moon, Jun Hwan, Eunjin Jeong, Seunghyun Kim, Taesoon Kim, Eunsoo Oh, Keun Lee, Hauk Han, and Young Keun Kim. "Materials quest for advanced interconnect metallization in integrated circuits." *Advanced Science* 10, no. 23 (2023): 2207321.

[43]. Fan, Dongxu, Weisheng Li, Hao Qiu, Yifei Xu, Si Gao, Lei Liu, Taotao Li et al. "Two-dimensional semiconductor integrated circuits operating at gigahertz frequencies." *Nature Electronics* 6, no. 11 (2023): 879-887.

[44]. Nemu, Ankita, Sangeeta Singh, Kamal K. Jha, Neha Tyagi, and Neeraj K. Jaiswal. "First-principles design of high speed nanoscale interconnects based on GaN nanoribbons." *Computational Materials Science* 249 (2025): 113625

[45]. Krishna, M. Sankush, Sangeeta Singh, and Brajesh Kumar Kaushik. "Planar quasi-1D nano-interconnects based on selective edge passivated ZnO nanoribbons." *IEEE Transactions on Nanotechnology* 22 (2023): 597-605.

[46]. Jatkar, Mandar, and P. Y. Mallikarjun. "Optimized Cu/Fe doped Boron Nitride Nanoribbons as nanoscale interconnect: DFT Investigation." *Materials Science in Semiconductor Processing* 186 (2025): 109050.

[47]. Jatkar, Mandar, Kamal K. Jha, and Sarat K. Patra. "First-principles investigation of F-functionalized ZGNR/AGNR for nanoscale interconnect applications." *Journal of Computational Electronics* 20, no. 4 (2021): 1461-1470.

[48]. International Technology Roadmap for Semiconductors, 2007 edition, https://www.semiconductors.org/wp-content/uploads/2018/08/2007Interconnect.pdf (accessed 27-11-2025).